The Cryosphere

Open Access

Glacier-surge mechanisms promoted by a hydro-thermodynamic feedback to summer melt

T. Dunse[1], T. Schellenberger[1], J. O. Hagen[1], A. Kääb[1], T. V. Schuler[1], and C. H. Reijmer[2]

[1]Department of Geosciences, University of Oslo, P.O. Box 1047, Blindern, 0316 Oslo, Norway
[2]Institute for Marine and Atmospheric Research Utrecht, Utrecht University, Princetonplein 5, 3584 CC Utrecht, the Netherlands

Correspondence to: T. Dunse (thorben.dunse@geo.uio.no)

Abstract. Mass loss from glaciers and ice sheets currently accounts for two-thirds of the observed global sea-level rise and has accelerated since the 1990s, coincident with strong atmospheric warming in the polar regions. Here we present continuous GPS measurements and satellite synthetic-aperture-radar-based velocity maps from Basin-3, the largest drainage basin of the Austfonna ice cap, Svalbard. Our observations demonstrate strong links between surface-melt and multiannual ice-flow acceleration. We identify a hydro-thermodynamic feedback that successively mobilizes stagnant ice regions, initially frozen to their bed, thereby facilitating fast basal motion over an expanding area. By autumn 2012, successive destabilization of the marine terminus escalated in a surge of Basin-3. The resulting iceberg discharge of $4.2 \pm 1.6\,\mathrm{Gt\,a^{-1}}$ over the period April 2012 to May 2013 triples the calving loss from the entire ice cap. With the seawater displacement by the terminus advance accounted for, the related sea-level rise contribution amounts to $7.2 \pm 2.6\,\mathrm{Gt\,a^{-1}}$. This rate matches the annual ice-mass loss from the entire Svalbard archipelago over the period 2003–2008, highlighting the importance of dynamic mass loss for glacier mass balance and sea-level rise. The active role of surface melt, i.e. external forcing, contrasts with previous views of glacier surges as purely internal dynamic instabilities. Given sustained climatic warming and rising significance of surface melt, we propose a potential impact of the hydro-thermodynamic feedback on the future stability of ice-sheet regions, namely at the presence of a cold-based marginal ice plug that restricts fast drainage of inland ice. The possibility of large-scale dynamic instabilities such as the partial disintegration of ice sheets is acknowledged but not quantified in global projections of sea-level rise.

1 Introduction

Glacier mass loss constitutes the largest contributor to global mean sea-level rise (SLR), followed by ocean thermal expansion (Church et al., 2011). Over the last two decades, both glaciers and ice caps (Gardner et al., 2013), as well as ice sheets, have lost mass at accelerating rates (AMAP, 2011; Shepherd et al., 2012). These ice mass changes coincide with atmospheric warming that causes record summer temperatures and glacier melt in the Arctic (Gardner et al., 2011) and across the Greenland Ice Sheet (Tedesco et al., 2013). In addition to mass loss by melting, glacier dynamics have the potential to significantly amplify glacier response to climate change by altering the ice discharge to the ocean. Acceleration of outlet glaciers of the Greenland Ice Sheet are generally attributed to hydraulic lubrication and marine terminus destabilization by oceanic warming and calving (Nick et al., 2009; Bartholomew et al., 2010; Moon et al., 2014). West Antarctic ice-stream acceleration is generally attributed to reduced buttressing by thinning or loss of ice shelves (Shepherd et al., 2012). Recent observations of sustained ice flow and mass loss from northeastern Greenland and West Antarctica are also reported as evidence of a marine ice-sheet instability (Khan et al., 2014; Mouginot et al., 2014). This phenomenon, also known as tidewater-glacier instability, refers to glacier speed-up due to terminus retreat into deeper water (Meier and Post, 1987; Pfeffer, 2007).

To date, glacier-dynamic feedback processes remain poorly constrained and are therefore not yet incorporated in global projections of future glacier mass loss (IPCC, 2013). SLR projections released with the IPCC Fifth Assessment Report range from 0.26 to 0.82 m over the 21st century (IPCC, 2013). The projections include ice discharge from

the ice sheets into the ocean, however, based on current rates and not accounting for a future dynamic response to climate change. The IPCC acknowledges but is not able to quantify the probability of significantly higher SLR, such as that associated with disintegration of marine-based sectors of the Antarctic Ice Sheet (IPCC, 2013).

Variations in glacier flow, and hence ice discharge, encompass wide ranges of timescales and magnitudes, from diurnal velocity fluctuations to century-scale surge-type behaviour, and are mainly attributed to changes in basal drag (Clarke, 1987). Cyclic surge-type behaviour is thought to arise from internal instabilities (Meier and Post, 1969), whereas seasonal velocity variations are externally controlled by surface-melt-induced acceleration through basal lubrication (Iken and Bindschadler, 1986; Schoof, 2010; Hewitt, 2013). Basal water pressure, and thus basal drag, is controlled by the rate of water supply to the glacier bed and the capacity of the subglacial drainage system to accommodate increased discharge (Schoof, 2010). Increased meltwater supply may thus accelerate but also slow down ice flow if it facilitates the establishment of a hydraulically efficient drainage system (Schoof, 2010). Several recent studies therefore suggest that hydraulic lubrication alone has a more limited effect on the future net mass balance of the Greenland Ice Sheet (Nick et al., 2013; Shannon et al., 2013) than previously anticipated (Zwally et al., 2002). However, the two recent assessments do not account for changes in the extent of the basal area subjected to hydraulic lubrication or do not quantify changes in calving loss.

The effect of surface meltwater on the thermal structure of glaciers has only recently been considered in modelling studies and was termed cryo-hydrological warming (CHW; Phillips et al., 2010, 2013). CHW includes latent heat released during refreezing of meltwater, as well as direct heat transfer between water and ice. CHW has the potential to change englacial and basal temperatures within years, whereas changes in basal thermal regime by heat conduction alone would require decades to centuries (Phillips et al., 2010). Phillips et al. (2010) regard CHW as a phenomenon specific to the ablation area and suggest that more areas of the Greenland Ice Sheet will be subjected to CHW in the case of sustained climate warming and thus upward migration of the equilibrium-line altitude (ELA). CHW has the potential to enhance ice deformation through the temperature dependency of the ice viscosity (Phillips et al., 2010), as well as basal motion, if it were to increase the extent of the basal area at the pressure-melting point (Phillips et al., 2013). It has previously been suggested that present outlet glaciers may accelerate significantly if meltwater drainage to the bed were to spread inland (Alley et al., 2008; Bartholomew et al., 2011). Phillips et al. (2013) simulated ice dynamics within the wet snow zone of western Greenland. They achieved a best fit with an observed increase in wintertime velocities if both changes in englacial and basal temperatures, and hence ice deformation and basal motion, were considered.

Cyclic surge-type behaviour is an extreme example of variations in glacier flow, and characterized by long quiescent phases (decades to centuries) with slow ice flow followed by short-lived active phases (months to years) with orders-of-magnitude increases in flow velocities (Raymond, 1987; Dowdeswell et al., 1991). Resistance to sliding during the quiescent phase leads to build-up of an upper reservoir (Clarke et al., 1984). During a surge, mass is transferred from the reservoir area to a lower receiving area, often associated with kilometre-scale advances of the terminus and greatly enhanced calving flux in the case of tidewater glaciers (Murray et al., 2003a). Glacier surges are generally regarded as internal instabilities, and not thought to be driven by external factors (Meier and Post, 1969). Nevertheless, the climatic mass balance influences the build-up of the reservoir area and thus surge occurrence and periodicity (Dowdeswell et al., 1995). In addition, external factors may drive feedback processes that lead to amplified dynamic response, pushing the glacier towards an instability threshold.

On Svalbard, glacier surges are thought to be controlled by a thermally controlled soft-bed surge mechanism (Hamilton and Dowdeswell, 1996; Jiskoot et al., 2000; Murray et al., 2000, 2003b), as previously proposed for surges of polythermal glaciers in subpolar environments (Robin, 1955; Clarke, 1976; Clarke et al., 1984). This theory concerns the slow adjustment of the basal thermal regime and driving stresses in response to geometric changes during the quiescent phase, ultimately leading to a thermal switch from cold to temperate basal conditions, permitting for fast basal motion. Basal melting sets in and then subglacial till, if present, is thawed and its shear strength reduced by rising pore-water pressure, destabilizing the glacier and initiating the surge (Clarke et al., 1984; Tulaczyk et al., 2000). Dynamic thinning and reduction in surface slope reduce the driving stress and sliding rates, eventually bringing the surge to a halt (Clarke et al., 1984).

Thermal models of glaciers generally account for heat conduction through the ice, heat transfer by ice advection, and strain heating and frictional heating. The geothermal heat flux and the annual air temperature (plus firn warming) form the lower and upper boundary conditions, respectively. Thermal effects by water flow within glaciers have previously been mentioned and considered important (e.g. Clarke, 1976), but only recently has "cryo-hydrologic warming (CHW)" been put back into focus (Phillips et al., 2010, 2013). Clarke (1976) neglected CHW in thermal models of glacier surges by assuming that water flow within cold ice is limited. However, recent studies suggest meltwater connections from the surface to the bed through cold ice of substantial thickness (e.g. Das et al., 2008; Clason et al., 2014).

Direct observations of ice dynamics during glacier surges are scarce. The evolution of several surges on Svalbard was reconstructed from archived satellite radar data only after a surge was noticed. Snapshot velocities were derived preferably for the winter season, i.e. when surface melt is absent,
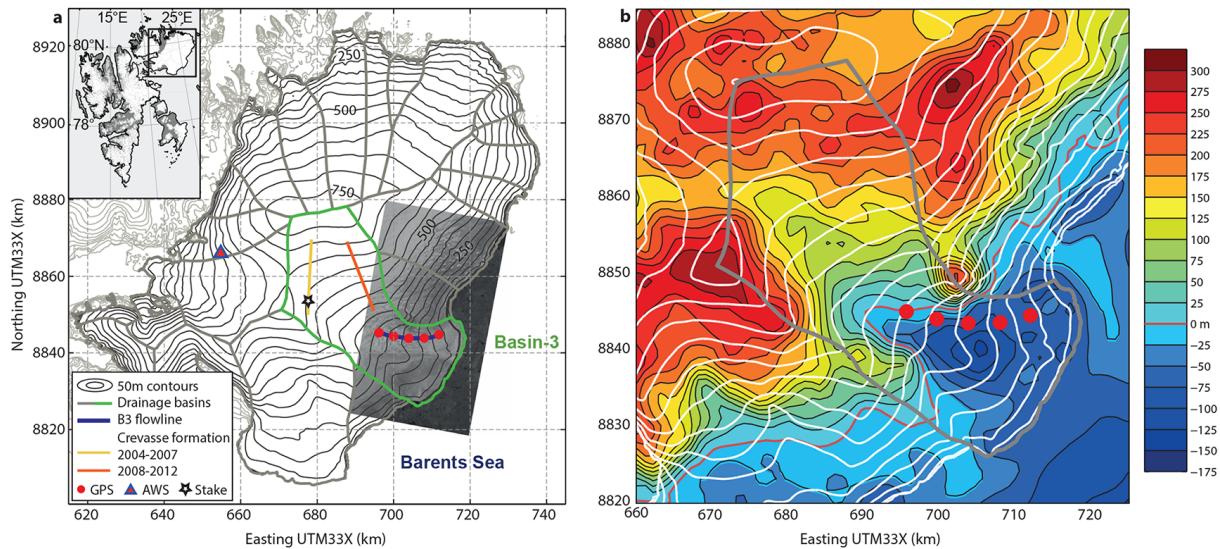
Figure 1. Surface and bedrock topography of Austfonna/Basin-3. **(a)** Surface elevation contours at 50 m interval (solid black), overlain on a TerraSAR-X backscatter image (30 April 2012). The insert provides the ice cap's location within the Svalbard archipelago. Drainage basins are outlined in solid grey; Basin-3 is outlined in solid green. The positions of five GPS receivers and one stake on Basin-3, as well as the automatic weather station (AWS), are marked. Repeat-GPR profiling revealed crevasse formation in upper reaches of Basin-3 between 2004 and 2007 and between 2008 and 2012 (Appendix D). **(b)** Bedrock contours (black, colour-filled) are at 25 m intervals, with the bedrock sea-level contour highlighted in red and 50 m surface elevation contours superimposed (white).

as liquid water deteriorates the quality of the derived motion maps using satellite interferometric radar (Luckman et al., 2002; Murray et al., 2003b, a). Changes in ice dynamics specifically during the summer melt season have therefore not been captured. Based on the available motion snapshots, Murray et al. (2003b) proposed that Svalbard glacier surges are characterized by gradual acceleration over several years, at a higher rate during the months towards the peak of the surge, and followed by multiannual, gradual slow-down.

Here, we present a 5-year record of continuous GPS measurements (May 2008 to May 2013) and satellite synthetic-aperture-radar-based velocity maps (since April 2012) from Basin-3, a marine-terminating drainage basin of the Austfonna ice cap on Svalbard. Our observations demonstrate strong links between surface-melt and ice-flow acceleration, culminating by October 2012 in a surge and drastically enhanced ice discharge. To date (January 2015), the surge continues. We propose a hydro-thermodynamic feedback mechanism to surface melt, subsequently mobilizing the ice within the reservoir area and weakening cold-based marginal ice that restricts inland ice from draining into the ocean. Finally, we discuss possible implications of the proposed mechanism for the stability of marine ice-sheet regions if exposed to significant surface melt in a warming climate.

2 Austfonna, Basin-3

At $\sim 7800\,\mathrm{km}^2$, Austfonna is the largest ice cap in the Eurasian Arctic (Fig. 1a). The ice cap consists of a main

dome with an ice thickness of up to 600 m that feeds a number of drainage basins, some of which are known to have surged in the past (Dowdeswell, 1986). Austfonna has a poly-thermal structure. In the ice cap's interior, basal temperatures are likely at the pressure-melting point (Zagorodnov et al., 1989), while the thinner ice-cap margins are cold and frozen to the bed, except for distinct fast-flowing outlets that are dominated by fast basal motion and imbedded within the generally slowly deforming ice cap (Dowdeswell et al., 1999). The southeastern basins are to a large extent grounded below sea level, and form a continuous, non-floating calving front towards the Barents Sea (Dowdeswell et al., 2008). The regions grounded below sea level are at least partially underlain by marine sediments (Dowdeswell et al., 2008). Over 2002–2008, the climatic mass balance of Austfonna was close to zero (Moholdt et al., 2010a). Yet the ice cap was losing mass due to calving and retreat of the marine ice margin that accounted for $2.5\,\mathrm{Gt\,a^{-1}}$ or $33 \pm 5\,\%$ of the total ablation (Dowdeswell et al., 2008).

Basin-3 ($\sim 1200\,\mathrm{km}^2$ and a length of $\sim 60\,\mathrm{km}$) is the largest drainage basin of Austfonna and topographically constrained by a subglacial valley that extends from south of the main dome eastwards towards the Barents Sea (Fig. 1b). About one-third of the ice base is grounded below sea level down to a maximum depth of $\sim 150\,\mathrm{m}$ within an overdeepening in the central terminus region (Fig. 1b; Dowdeswell et al., 1986; Dunse et al., 2011). A previous velocity map based on satellite radar interferometry from data acquired in the mid-1990s revealed an ice stream in the northern

lower reaches of Basin-3 with flow velocities $\leq 200\,\mathrm{m\,a^{-1}}$ (Dowdeswell et al., 2008). The ice stream was topographically constrained by a subglacial mountain to the north (Isdomen) and near-stagnant ice, likely frozen to its bed, to the south. The absence of surface lineations (e.g. crevasses) as late as 1991 identified the ice stream of Basin-3 as a recent feature (Dowdeswell et al., 1999). During the 1990s, the front retreated on average by $70 \pm 10\,\mathrm{m\,a^{-1}}$, accounting for two-thirds of the calving flux of $\sim 0.4\,\mathrm{Gt\,a^{-1}}$ (Dowdeswell et al., 2008). Basin-3 is known to have surged some time prior to 1870 (Lefauconnier and Hagen, 1991), and the advancing terminus created a pronounced surge lobe nearly 25 km in width. The terminal moraine associated with the last surge lies ~ 8 km from the present-day position of the calving front (Robinson and Dowdeswell, 2011). Based on lobe volume and accumulation rate, the duration of the quiescent phase of Basin-3 was estimated to last 130–140 years (Solheim, 1991), a very good estimate considering the basin's renewed surge activity since autumn 2012, which is reported on here.

3 Methods

3.1 Velocity time series

In spring 2008, five GPS receivers were deployed along the mid-1990s central flowline, 5 to 21 km upglacier from the calving front (Fig. 1; Dunse et al., 2012). We used GPS single-frequency code receivers (L1 band, C/A code only). Geographical positions were logged at hourly intervals, and every third hour for instruments installed after May 2011, at an accuracy typically better than 2 m (den Ouden et al., 2010). Filtering in the time domain was applied to reduce random errors, i.e. a 7-day running mean was applied to the daily mean position, velocities were computed, and, finally, the velocity was smoothed by applying another 7-day running mean (Dunse et al., 2012).

3.2 Velocity maps from synthetic aperture radar

Velocity maps of Basin-3, Austfonna, were produced from twenty-four 2 m resolution TerraSAR-X (TSX) scenes acquired between April 2012 and November 2013 and provided by the German Aerospace Center (DLR). Displacement fields were derived by using cross-correlation between two consecutive acquisitions (Strozzi et al., 2002) and geocoded using a DEM of Austfonna (Moholdt and Kääb, 2012). Appendix A provides more detailed information on the TSX data and processing. Calving front outlines were digitized from geocoded backscatter images (Appendix B). The calving flux of Basin-3 was derived by the ice flux through a fixed fluxgate upglacier of the calving front and the area change downglacier of that fluxgate, multiplied by an average ice thickness. The ice thickness was derived by differencing of a bedrock map (Fig. 1b; Dowdeswell, 1986;

Dunse et al., 2011) and a digital elevation model (Moholdt and Kääb, 2012).

3.3 Additional data

To approximate timing and magnitude of surface-melt periods, cumulative positive-degree days (PDD) were computed from the temperature record of an automatic weather station. The station has operated since April 2004 on the western flank of Austfonna at $22°25'12''$ E, $79°43'48''$ N and 370 m a.s.l. (Schuler et al., 2014). Surface crevasses were identified and mapped using ground-penetrating radar (Ramac GPR; Målå Geoscience) at a centre frequency of 800 MHz, providing structural information from the glacier surface down to a depth of ~ 12 m (Dunse et al., 2009, Appendix C). GPR profiles were annually repeated subsequent to 2004 and geolocated using a kinematic global navigation satellite system (GNSS; GPS and GLONASS).

4 Results

4.1 Multiannual ice-flow acceleration

Winter velocities observed by GPS in May 2008 were significantly higher than in the mid-1990s (Fig. 2). The GPS time series also reveal considerable overall acceleration, occurring in pronounced steps, each of which coincides with the summer melt period, as indicated by the temperature record of an automatic weather station (Fig. 2; Schuler et al., 2014). The 2008 summer speed-up is followed by a gradual winter deceleration. In total, 60–95 % of the velocity increase during summer is reversible (Appendix D). However, during subsequent years, an increasing fraction of the summer speed-up is of lasting nature, i.e. increased summer velocities are sustained throughout the winter although surface melt had ceased.

Multiannual changes in ice dynamics are also evident from within the reservoir area, higher up on Basin-3. The annual position change of a mass-balance stake close to the ice divide (Fig. 1) revealed strong acceleration from $11\,\mathrm{m\,a^{-1}}$ between 2004 and 2007 to 28, 43 and $114\,\mathrm{m\,a^{-1}}$ for the period 2010–2013. In addition, annually repeated GPR surveys reveal first and cumulative occurrence of surface crevasses from ~ 2004 onwards, between ~ 2004 and 2007 along the western profile, and between 2008 and 2012 along the eastern profile (Fig. 1a; Appendix C).

4.2 Mobilization of stagnant ice regions

The drastic acceleration during autumn 2012 coincided with the expansion of the fast-flowing region across the entire basin, as revealed by a time series of ice-surface velocity maps based on intensity tracking of repeat-pass TerraSAR-X satellite radar images (Fig. 3; Appendix B). Velocities in April 2012 were up to $3\,\mathrm{m\,d^{-1}}$, 1 order of magnitude larger
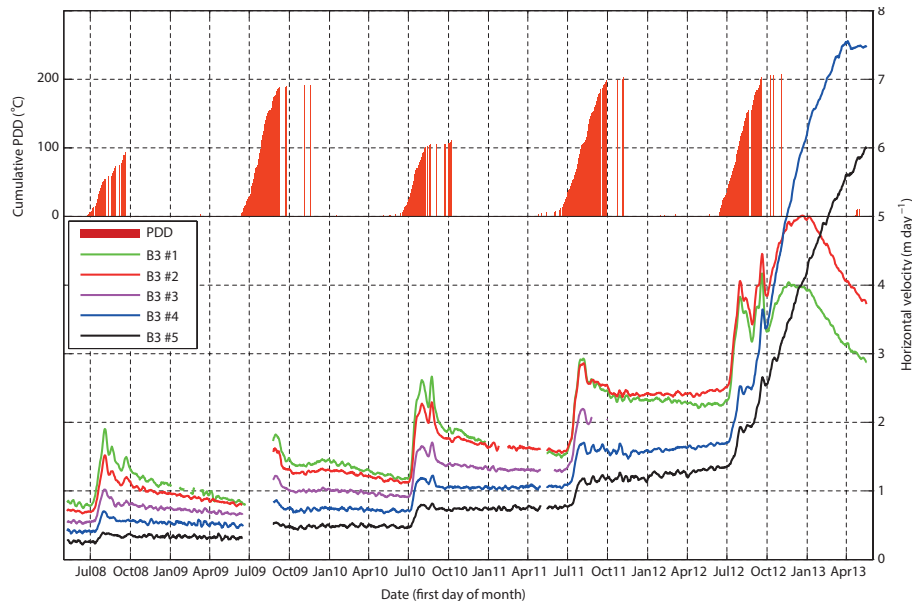
Figure 2. Flow velocities along the centreline of the fast-flow region of Basin-3, Austfonna, between May 2008 and May 2013. GPS stations are numbered from 1 at the lowest elevation to 5 at the highest (Fig. 1). Red bars (upper panel) indicate potential melt days and cumulative positive-degree days (PDD) for each summer, inferred from the temperature record of an automatic weather station.

than in the mid-1990s (Fig. 3a). In April 2012, the fast-flow region extended farther inland and had widened southward to a width of ~ 6–$8\,\mathrm{km}$, as compared to ~ 5–$6\,\mathrm{km}$ in the mid-1990s. As a result of southward expansion, the GPS receivers were located $\sim 1\,\mathrm{km}$ north from the central flow-line and did not capture fastest flow velocities. In contrast to the mid-1990s, the southeastern corner of Basin-3 also displayed fast motion, at velocities of up to $1\,\mathrm{m\,d^{-1}}$. These two distinct fast-flow regions were completely separated by almost stagnant ice, notably including the calving front. Low ice velocities, $< 0.1\,\mathrm{m\,d^{-1}}$, indicate the absence of considerable basal motion, and suggest frozen-bed conditions in this region. In August 2012, i.e. at the end of the summer melt season, velocities had increased significantly, up to $6\,\mathrm{m\,d^{-1}}$ for the northern and $4\,\mathrm{m\,d^{-1}}$ for the southeastern fast-flow region, along with further lateral expansion of the fast-flowing areas. Consequently, the slow-moving ice region in between had decreased in size (Fig. 3b) and disappeared by October 2012, when ice flow escalated into a surge comprising the entire width of the basin, reaching velocities $> 10\,\mathrm{m\,d^{-1}}$ (Fig. 3c). Velocities increased further until January 2013, reaching a maximum of $20\,\mathrm{m\,d^{-1}}$ (Fig. 3d). Between January and May 2013 the maximum velocities decreased to $15.2\,\mathrm{m\,d^{-1}}$, while the upglacier regions continued to accelerate (Fig. A1b). By the end of 2013, fast flow of Basin-3 continued (Appendix A).

4.3 Calving flux

The TSX data allowed for calculation of the calving flux components, i.e. (i) the ice flux through a fixed fluxgate near

the calving front, and (ii) the mass change of the terminus downglacier of that fluxgate, accounting for front position changes (Fig. 4; Appendix B). The observed ice flux peaked at a rate of $13.0 \pm 4.2\,\mathrm{Gt\,a^{-1}}$ in December 2012/January 2013, after which it decreased slightly (Fig. 4a). Prior to October 2012, the position of the entire calving front of Basin-3 was remarkably stable (slight retreat; Fig. 4b), indicating that the entire ice flux was balanced by iceberg calving. After November 2012, the southern and central parts of the front advanced by $> 1\,\mathrm{km}$, reducing ice mass loss through calving by 61 %, as compared to a stable front position.

Direct conversion of calving mass loss to SLR contribution is only meaningful for a static calving front. Glacier surges are typically accompanied by significant terminus advances. An advancing terminus reduces the mass loss from the glacier; however, the submerged part of the terminus replaces sea water instantaneously, causing an instantaneous sea-level rise. We therefore distinguish between a glacier mass balance and a sea-level perspective on the calving flux (Fig. 4c; Table 1). From 19 April 2012 to 9 May 2013, calving mass loss [yearly rate] from Basin-3 accounted for $4.4 \pm 1.6\,\mathrm{Gt}$ [$4.2 \pm 1.6\,\mathrm{Gt\,a^{-1}}$], an increase by an order of magnitude compared to 1991–2008 (Dowdeswell et al., 2008), nearly tripling the calving loss from the entire Austfonna ice cap. The related sea-level rise contribution of $7.6 \pm 2.7\,\mathrm{Gt}$ [$7.2 \pm 2.6\,\mathrm{Gt\,a^{-1}}$] is as large as the total glacier mass change from the entire Svalbard archipelago for the period 2003 to 2008, estimated to be $-6.6 \pm 2.6\,\mathrm{Gt\,a^{-1}}$ (Moholdt et al., 2010b). Rates of sea-level rise contribution are expected to decline once the surge of Basin-3 has terminated, i.e. once the
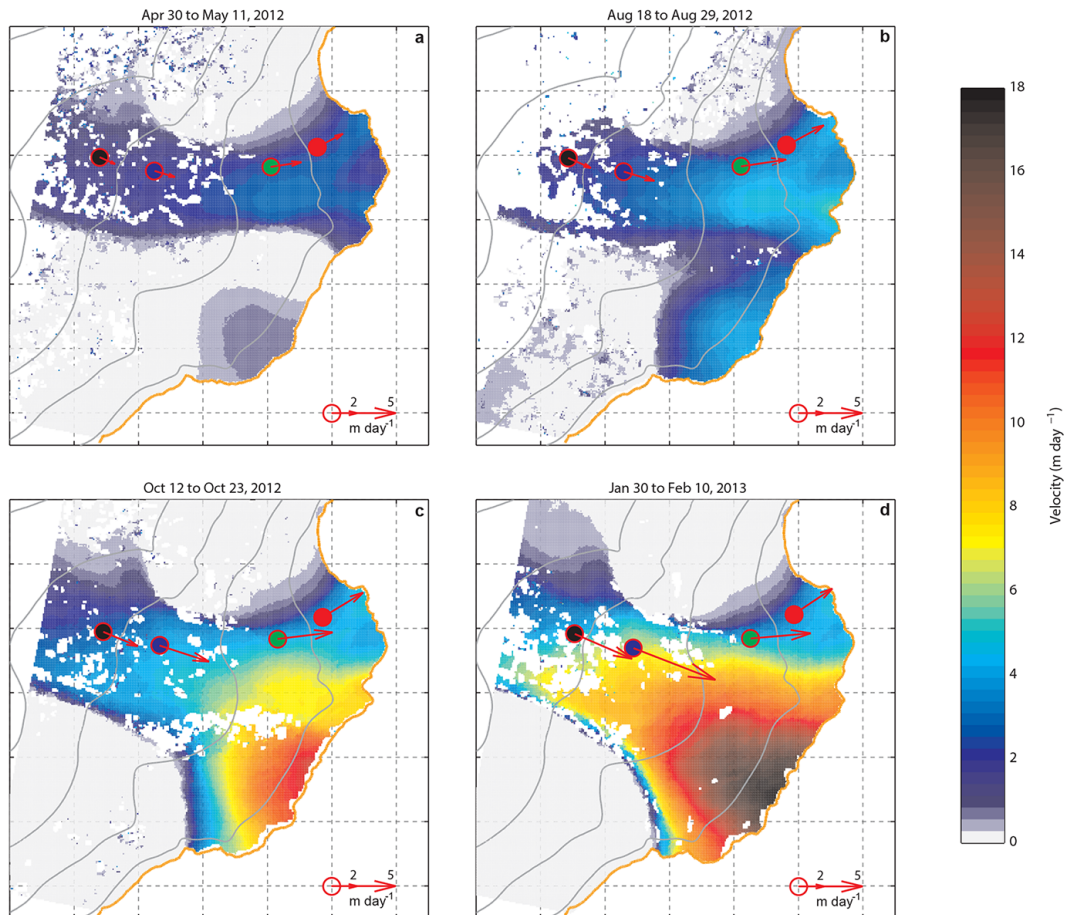
Figure 3. Surface velocity fields of Basin-3, Austfonna, derived from TerraSAR-X feature tracking: **(a)** April/May 2012, **(b)** August, **(c)** October, and **(d)** January/February 2013. Red circles represent mean position of GPS receivers over the particular repeat-pass period; fill colour according to colour coding of receivers in Fig. 2. The red arrows indicate associated GPS velocity vectors. Glacier elevation contours plotted in grey at 100 m intervals; front position at time of repeat pass in orange.

ice flux has diminished and the terminus advance has come to a halt. Nevertheless, iceberg calving and hence ice mass loss will be maintained, depending on future rates of marine-terminus retreat.

5 Discussion

The dynamic changes that have been observed at Basin-3 over the last two decades can be separated into three phases: (1) activation of a spatially confined fast-flow region in the early 1990s (Dowdeswell et al., 1999), (2) multiannual acceleration and expansion of the fast-flow region from < 2008 to 2012, and (3) active surge phase following the destabilization of the entire terminus in autumn 2012.

5.1 Phase 1: Initiation of spatially confined fast flow

Spatially confined fast flow was initiated in the northern part of lower Basin-3 in the early 1990s, and interpreted as a temporary flow instability (Dowdeswell et al., 1999). Activation of fast flow within this region could be explained by internal mechanisms, i.e. by gradual changes in basal thermal regime and driving stress, associated with long-term geometric changes during the quiescent phase (e.g. Clarke, 1976; Clarke et al., 1984). Numerical simulations of Austfonna support the concept of a thermally controlled soft-bed surge mechanism (Dunse et al., 2011), as proposed earlier for Svalbard glacier surges (Hamilton and Dowdeswell, 1996; Jiskoot et al., 2000; Murray et al., 2000, 2003b). Spatially confined fast flow since the early 1990s entailed an ice flux in excess of the balance flux (Dowdeswell et al., 1999) and thus a drawdown of the reservoir area. Extensional flow within the reservoir area is expected to form crevasses (van der Veen, 1999), as indeed observed by GPR since ∼ 2004 (Fig. 1a; Appendix C).
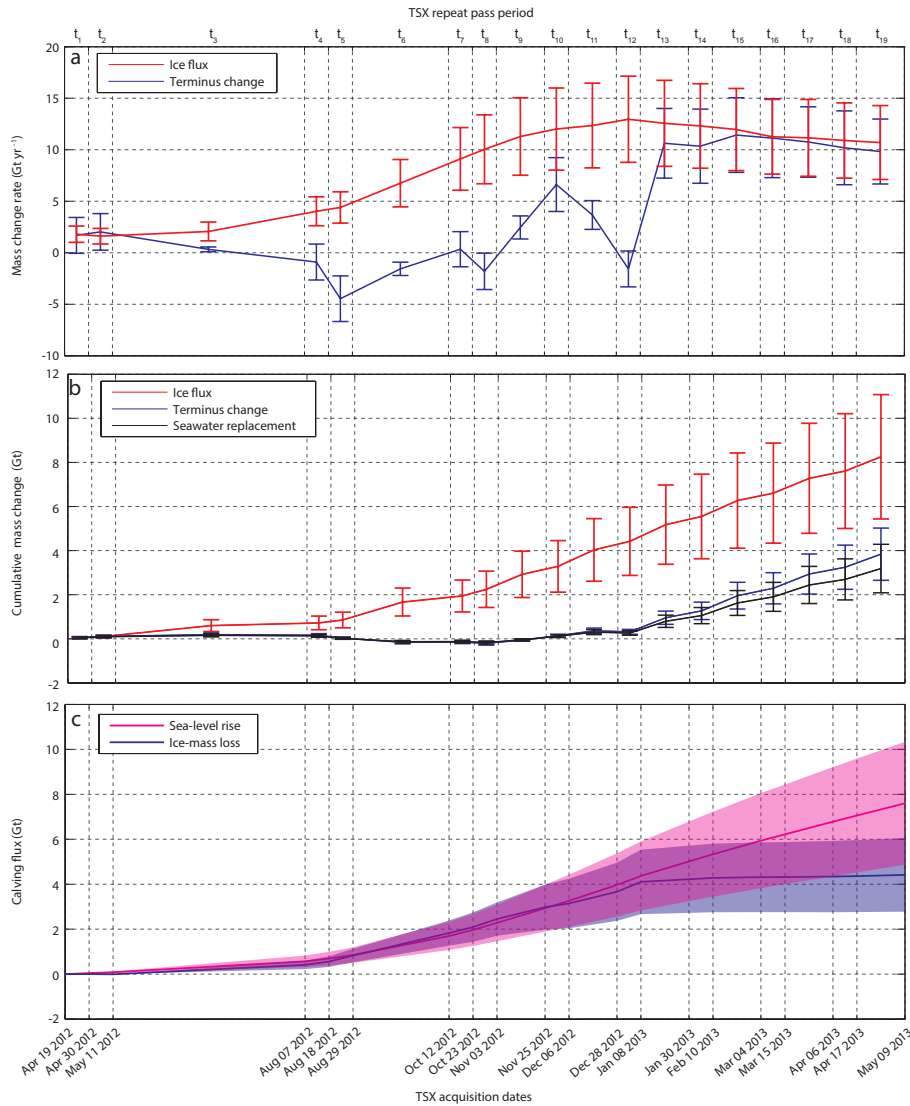
Figure 4. Calving flux from Basin-3, Austfonna, April 2012 to May 2013. Calving components are expressed in terms of the instantaneous **(a)** and cumulative mass change **(b)** and allocated to the effect on glacier mass balance and sea level **(c)** (see Sect. 4.3). Whiskers in **(a, b)** indicate uncertainty bounds calculated using propagation-of-uncertainty analysis, and shaded areas in **(c)** indicate upper and lower bounds given maximum or minimum ice thickness.

Table 1. Estimate of calving flux components and total calving flux over the TSX observation period from 19 April 2012 to 9 May 2013.

Calving flux components	(Gt)	(Gt a^{-1})
Ice flux, Q_{fg}	8.3 ± 2.8	7.8 ± 2.7
Terminus change, Q_t	3.8 ± 1.2	3.6 ± 1.1
Terminus-seawater displacement, Q_{tsd}	3.2 ± 1.1	3.0 ± 1.0
Total calving flux		
Mb perspective, $Q_{mb} = Q_{fg} - Q_t$	4.4 ± 1.6	4.2 ± 1.5
SLR perspective, $Q_{sl} = Q_{mb} + Q_{tsd}$	7.6 ± 3.9	7.2 ± 2.6

5.2 Phase 2: Mobilization of the reservoir – multiannual, stepwise acceleration

The multiannual acceleration of Basin-3, observed by GPS since 2008, occurred in discrete steps, each of which coincident with consecutive summer melt periods (Fig. 2). The high sensitivity and short response time (days) of glacier dynamics to melt events clearly suggest surface-melt-triggered acceleration. Short-lived acceleration during the melt season is consistent with current understanding of hydraulic lubrication (Schoof, 2010). In contrast, the multiannual acceleration of background velocities (Appendix D) cannot be explained by this mechanism and suggests a fundamental change in dynamics.

Enhanced post-summer velocities sustained throughout the winter can be explained by successive activation of previously stagnant ice regions during the previous summer melt period. Mobilization of increased ice volumes within the reservoir area leads to increased velocities and discharge. A widening of the fast-flow region itself allows for higher centreline velocities due to the increased distance from the lateral shear margin, analogous to the behaviour of Antarctic ice streams (Joughin and Alley, 2011).

Mobilization of the reservoir area is evident from the surface-crevasse formation within the upper accumulation area of Basin-3 since ∼ 2004 (Fig. 1a; Appendix C). Crevasses are a manifestation of longitudinal extension and evidence of upglacier migration of the fast-flowing region. This is in line with the upglacier expansion of the ice stream revealed by TSX and the observed strong acceleration of the mass-balance stake within the reservoir area (Fig. 1). The first occurrence of crevasses signifies the development of potential meltwater routes to the glacier bed, subjecting an increasing region to CHW and basal hydraulic lubrication. Similarly, meltwater reaching the bed beneath the heavily crevassed shear margin of the fast-flow region efficiently weakens the basal drag that balances the lateral drag, which in turn regulates ice velocities (Joughin and Alley, 2011). CHW and increased frictional heating both act to enhance this mechanism, weakening the flow resistance exerted by the lateral shear margins and possibly cold-based ice patches acting as "sticky spots" (Alley, 1993). The interplay between CHW and the emergence of basal hydraulic lubrication over an expanding area of the ice base constitutes a hydro-thermodynamic feedback. Unconsolidated subglacial sediments underneath the marine-based ice of Basin-3 act to further enhance this feedback. Input of surface meltwater during consecutive summers progressively raises the pore-water pressure within the sediment, reducing its shear strength and favouring rapid destabilization (Clarke et al., 1984; Tulaczyk et al., 2000).

5.3 Phase 3: Destabilization of the marginal ice plug – basin-wide surge

A surge comprising the full width of Basin-3 and the subsequent advance of the terminus followed the mobilization of the remaining stagnant ice regions, notably including the calving front. Water flow may have accessed the cold-ice base through partially unfrozen subglacial sediments, as suggested in the case of Trapridge Glacier, Yukon, Canada (Clarke et al., 1984). Field measurements of thermal structure and ice flow during a surge of Trapridge Glacier do not indicate that the cold ice below the surge front acts as a thermal barrier to water flow. Clarke et al. (1984) observed very high temperature gradients in the cold basal ice below a surge front, about 10 times larger than expected from geothermal heat flux, and attributed this to water flow through an unfrozen substrate beneath the cold ice. The abrupt onset of

fast flow in previously stagnant regions of Basin-3 suggests sheer tearing of the glacier from its bed. This activation was possibly related to a combination of warming of the glacier bed through CHW and mechanical stress transfer from active ice further upstream. During the fieldwork in spring 2012, large ice blocks were observed to be pushed upward above the glacier surface near the lower shear margin, an indication of strong longitudinal stresses.

While fast flow continued by the end of 2013, it is expected to slow down or come to a halt within a few years. Massive ice redistribution from the reservoir into the receiving area and towards the calving front efficiently lowers the driving stress. Eventually, temperate basal conditions underneath the dynamically thinned and decelerating terminus are expected to be no longer maintained, at which time the base of the ice will start to refreeze to its bed (Clarke et al., 1984; Dunse et al., 2011).

5.4 Hydro-thermodynamic feedback mechanism

We cannot explain our observations using standard theory of glacier surges alone (e.g. Clarke et al., 1984). The multiannual acceleration did not occur uniformly or gradually, as previously thought characteristic of Svalbard glacier surges (Murray et al., 2003b, a). Incorporating the effect of CHW over an expanding area of the glacier bed provides, we believe, a good explanation of our observations (Fig. 5). The hydro-thermodynamic feedback proposed here is not limited to CHW; it also includes the additional hydraulic lubrication effects. Ice regions undergoing a switch from cold to temperate basal conditions were previously characterized by frozen conditions, i.e. absence of water. In the initial stage of basal–hydraulic drainage system development, water input is likely to raise water pressure and enhance basal motion, in line with the established theory on basal lubrication (e.g. Schoof, 2010). In addition, thawing of underlying frozen till and rising pore-water pressure lead to enhanced sediment deformation. These processes all result in an enhancement of ice flow. Longitudinal extension opens new surface crevasses that provide englacial pathways for meltwater in subsequent summers, subjecting a larger region of the bed to surface melt. Eventually, the entire drainage basin is sufficiently destabilized, initiating the surge. Once the entire basin is moving by fast basal motion, i.e. the entire base is at pressure melting, and driving stresses are decreasing, the hydro-thermodynamic feedback no longer operates.

We would like to stress that the hydro-thermodynamic feedback proposed here does not oppose, but can be understood as an integral part of the theory of thermally controlled soft-bed glacier surges, as illustrated in Fig. 5. An increasing fraction of the glacier bed is subjected to surface melt, and basal processes conductive for surge behaviour are amplified. Basal processes include, in particular, (1) CHW that leads to a switch from cold to temperate basal conditions, permitting for fast basal motion; (2) expansion of the area
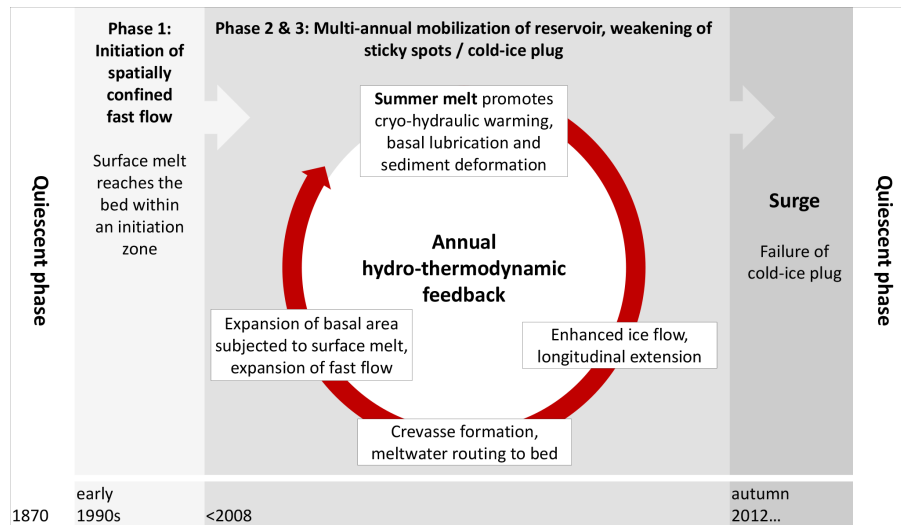
Figure 5. Schematic illustration of the proposed hydro-thermodynamic feedback to summer melt, imbedded within the surge cycle of Basin-3, Austfonna. The approximate start of each phase is indicated at the bottom. Phase 1 follows from long-term changes in glacier geometry, i.e. build-up of a reservoir, and associated changes in driving stress and basal thermal regime. The hydro-thermodynamic feedback loop operates over several years during phase 2 and 3, each loop coinciding with consecutive summer melt periods. Successive mobilization and destabilization initiates the surge. Dynamic thinning, reduction in driving stress and basal heat dissipation eventually terminate the surge.

subjected to basal lubrication; and (3) rising pore-water pressure and sediment deformation. The feedback requires an initiation zone in which surface meltwater can access the bed, such as the spatially confined fast-flow region described in phase 1. Alternatively, supra-glacial lake drainage may establish full ice-thickness meltwater pathways (Das et al., 2008). Our observations of Basin-3 suggest, on the one hand, a significant contribution of the hydro-thermodynamic feedback on the mobilization of the reservoir area and, on the other hand, weakening of the flow resistance within the receiving area.

5.5 Implications for the future stability of ice sheets

Surface melt has likely been a widespread phenomenon on Svalbard throughout most of the Holocene. The current surge of Basin-3 should therefore not be mistaken as a response to recent Arctic warming. The hydro-thermal feedback could also have played a role in previous Svalbard glacier surges. Given continued global warming, characterized by more widespread and intense occurrence of surface melt, we hypothesize that the hydro-thermodynamic feedback may gain importance in other glaciated regions, including the ice sheets.

Rapid marine ice-sheet disintegration is evident from geological records both in the Northern and Southern Hemisphere and typically associated with air temperatures similar to or warmer than those predicted for the end of the 21st century (Cook et al., 2013; Deschamps et al., 2012). Ice-rafted debris distributed across the North Atlantic ocean floor provides evidence of substantial calving associated with the

rapid disintegration of the Laurentide Ice Sheet, so-called Heinrich events (Bond et al., 1992). Palaeoclimatic records suggest rates of sea-level change much greater than currently observed or projected for the 21st century, e.g. 3.5 to 5 m SLR per century (35–50 mm a^{-1}) at the end of the Last Glacial Maximum, $\sim$ 14.5 ka ago (Deschamps et al., 2012).

Analogies between glacier surges and partial ice-sheet collapses are widespread throughout the glaciological literature (e.g. Clarke et al., 1984; Jiskoot et al., 2000). Analogous to the ice sheets, ice caps like Austfonna consist of slow-moving inland ice interspersed with faster-flowing outlet glaciers and ice streams that deliver inland ice towards the calving front. Drainage basins of Austfonna in their quiescent phase are characterized by margins frozen to their bed (Dowdeswell et al., 1999). Similarly, the coastal margins of the Antarctic Ice Sheet contain large regions of cold-based ice (Pattyn, 2010) that may currently prohibit efficient drainage of warm-based interior ice towards the ocean – e.g. in the Wilkes Basin, East Antarctica, which is known to have been dynamically active during the Pliocene warmth (Cook et al., 2013). A very recent model study confirms the potential dynamic instability of the Wilkes Basin, following the removal of a cold-ice plug (Mengel and Levermann, 2014). In that study, a retreat of the grounding line is forced by oceanic warming, thereby eliminating the cold-ice plug.

Our proposed mobilization of the reservoir area of Basin-3 is in line with Phillips et al. (2013), pointing at the potential of CHW in mobilizing more inland ice regions of the Greenland Ice Sheet, thereby increasing ice discharge through existing outlet glaciers. An obvious feature that distinguishes Basin-3 from Greenland outlet glaciers is the pres-

ence of a cold-based ice plug that, until autumn 2012, restricted drainage from the reservoir area. In the case of fast-flowing Greenland outlet glaciers, the thermo-dynamic feedback would therefore lead to gradual acceleration, as long as the ELA continues migrating upglacier, rather than leading to surge-type behaviour. In southwestern Greenland, further acceleration of Jacobshavn Isbræ followed the 2012 record summer melt season (Joughin et al., 2014). Although the authors attribute the acceleration to terminus retreat into a bedrock depression, the occurrence of pronounced summer speed-up at higher elevations may also reflect inland migration of surface melt and the effect of associated hydraulic feedbacks on glacier dynamics (Alley et al., 2008; Meierbachtol et al., 2013; Phillips et al., 2013). Similarly, the hydro-thermodynamic feedback may play a role in the sustained mass loss recently reported from northeastern Greenland and mainly attributed to sea-ice decline due to regional warming (Khan et al., 2014).

6   Summary and conclusion

For the first time, to our best knowledge, we have obtained continuous in situ velocity observations during glacier-surge initiation. Our observations from Basin-3 of Austfonna reveal details of a surge that have never been recorded before. Unlike proposed earlier for Svalbard glacier surges (Murray et al., 2003b, a), multiannual acceleration during surge initiation of Basin-3 was not gradual but occurred in discrete steps, coincident with successive summers. We propose a hydro-thermodynamic feedback mechanism triggered by surface melt reaching a growing fraction of the glacier bed. Intrusion of surface melt to the glacier bed provides an efficient heat source through CHW, facilitating a thermal switch from cold to temperate basal conditions, permitting for basal motion. Initiation of hydraulic lubrication, along with rising pore-water pressure within subglacial sediments, further enhances basal motion, eventually destabilizing the overlying ice. These processes have earlier been summarized as thermally controlled soft-bed surge mechanism (e.g. Clarke et al., 1984; Murray et al., 2003b). However, the active role of surface melt and the associated hydro-thermodynamic feedback mechanism contrast the previous understanding of glacier surges as purely internal instabilities.

The recent calving flux of Basin-3 has strong implications for the mass balance of the ice cap and its contribution to sea-level rise. From 19 April 2012 to 9 May 2013, the calving flux [yearly rate] of Basin-3 amounted to 4.4 ± 1.6 Gt [4.2 ± 1.6 Gt a^{-1}], an increase by an order of magnitude compared to 1991–2008 (Dowdeswell et al., 2008). With the terminus advance accounted for, the related sea-level rise contribution of 7.6 ± 2.7 Gt [7.2 ± 2.6 Gt a^{-1}] equals the total annual glacier mass loss from the entire Svalbard archipelago for the period 2003 to 2008, estimated to be 6.6 ± 2.6 Gt a^{-1} (Moholdt et al., 2010b).

Given continued climatic warming and increasing surface melt, we hypothesize that the hydro-thermodynamic feedback may gain significance in other glaciated areas, including the ice sheets. In light of recent record melt and rising ELA of the Greenland Ice Sheet, the proposed mechanism has the potential to lead to a long-term enhancement of outlet-glacier discharge and calving loss, as earlier proposed by Phillips et al. (2013). Our expectation contrasts with recent studies that indicate limited effects of surface-melt-induced acceleration on the future net mass balance of the Greenland Ice Sheet (Nick et al., 2013; Shannon et al., 2013). Surface melt in Antarctica is presently mainly constrained to the ice shelves (Comiso, 2000). Given strong continued warming, surface melt will increasingly occur over coastal areas of Antarctica, making the grounded ice-sheet margins vulnerable to the hydro-thermodynamic feedback.

Our study of the Austfonna ice cap highlights the importance of dynamic ice-mass loss for glacier mass balance. Current model projections of future SLR (IPCC, 2013) still do not account for the dynamic response of glaciers to continued global warming and might need to be revised upward after incorporating mechanisms such as CHW and the hydro-thermodynamic feedback.

Appendix A: TerraSAR-X velocity maps

Twenty-four TerraSAR-X (TSX) satellite synthetic aperture radar scenes of ∼ 2 m ground resolution (TSX Stripmap mode) were acquired between April 2012 and November 2013 (Table A1), providing information on the spatial evolution of the surge (Fig. 3). For each pair of consecutive acquisitions, displacements were determined using cross-correlation of the intensity images (Strozzi et al., 2002) and 21 velocity maps produced by accounting for the respective repeat-pass period (Table A1). The size of the matching window was adjusted according to the expected maximum displacements during the repeat pass cycle: 300×344 pixels in range and azimuth direction in the case of 11 days or 599×688 pixels for 22 days or longer. Displacements were measured in discrete steps of 50×57 pixels in range and azimuth to achieve a resolution of ∼ 100×100 m. Velocity maps were calculated from displacement maps by accounting for the time interval between the two underlying TSX images (t_1 to t_{21}, Table A1) and geocoded using a DEM of Austfonna (Moholdt and Kääb, 2012). Velocities larger than a carefully estimated maximum (Table A1) were classified as mismatches and removed. To estimate the ice flux (Appendix B), obvious erroneous velocities remaining in the vicinity of a fixed fluxgate were manually removed and the maps interpolated using inverse distance weighting to provide continuous velocity profiles along the fluxgate (Fig. A1a). A comparison between TSX and GPS velocities for each GPS station and all repeat-pass periods revealed that TSX underestimated local velocities at the GPS stations by $0.3 \, \mathrm{m \, d^{-1}}$ (Fig. A2). We explain this small bias by large horizontal velocity gradients within large matching windows, which could lead to the average velocities within a matching window being typically smaller than the strictly local GPS velocity. Consequently, more stable areas produce best matches.

Table A1. TerraSAR-X acquisitions of Basin-3 and repeat-pass period and maximum velocities of inferred velocity maps.

ID of period	Repeat-pass period (days)	Start and end-date	Maximum velocity ($\mathrm{m \, d^{-1}}$)
t_1	11	19 Apr 2012–30 Apr 2012	4.5
t_2	11	30 Apr 2012–11 May 2012	4.5
t_3	88	30 Apr 2012–7 Aug 2012	4.5
t_4	11	7 Aug 2012–18 Aug 2012	6.4
t_5	11	18 Aug 2012–29 Aug 2012	6.8
t_6	44	29 Aug 2012–12 Oct 2012	8.4
t_7	11	12 Oct 2012–23 Oct 2012	13.6
t_8	11	23 Oct 2012–3 Nov 2012	13.6
t_9	22	3 Nov 2012–25 Nov 2012	15.9
t_{10}	11	25 Nov 2012–6 Dec 2012	18.2
t_{11}	22	6 Dec 2012–28 Dec 2012	18.4
t_{12}	11	28 Dec 2012–8 Jan 2013	20.0
t_{13}	22	8 Jan 2013–30 Jan 2013	18.6
t_{14}	11	30 Jan 2013–10 Feb 2013	18.6
t_{15}	22	10 Feb 2013–4 Mar 2013	17.5
t_{16}	11	4 Mar 2013–15 Mar 2013	17.3
t_{17}	22	15 Mar 2013–6 Apr 2013	16.1
t_{18}	11	6 Apr 2013–17 Apr 2013	16.4
t_{19}	22	17 Apr 2013–9 May 2013	15.2
t_{20}	11	16 Aug 2013–27 Aug 2013	15.5
t_{21}	11	12 Nov 2013–23 Nov 2013	12.5
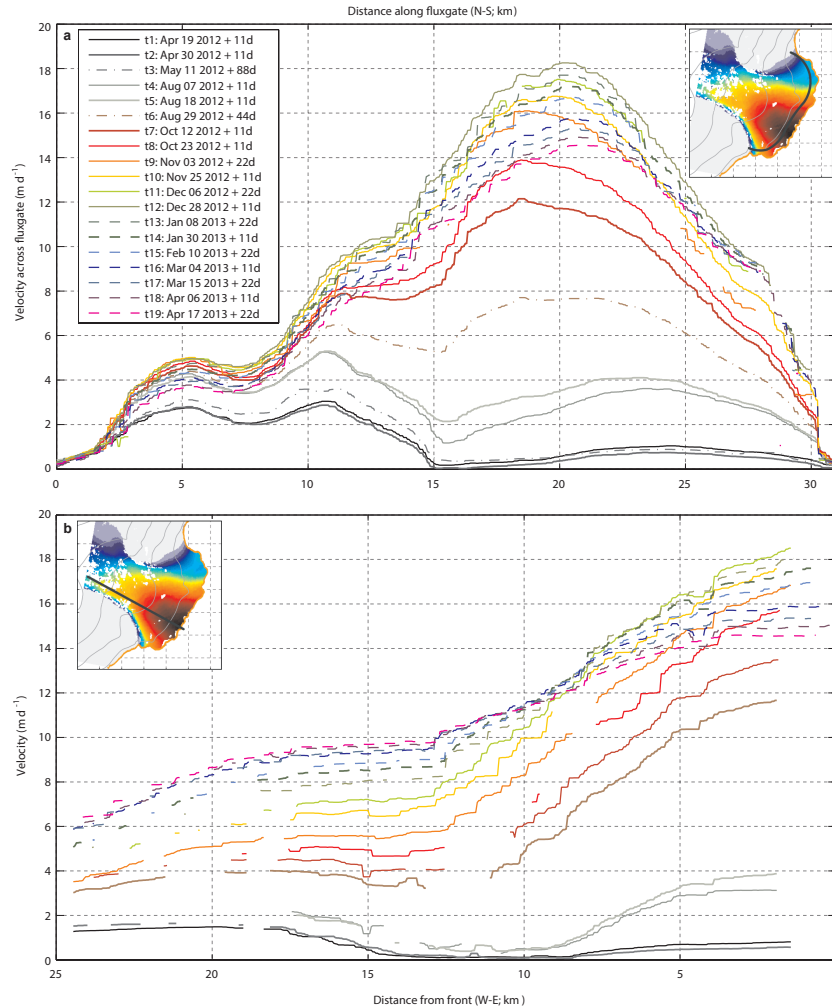
Figure A1. Evolution of ice-flow velocities across a calving fluxgate **(a)** and along a central flowline of Basin-3 **(b)**. Velocity profiles extracted from TerraSAR-X velocity maps April 2012 to May 2013 and median filtered to remove outliers. The insert shows the location of the profiles overlain onto the velocity map of t_{14}. Fluxgate velocities are used to compute the calving ice flux. Velocities for long repeat passes t_3 and t_6 have been constructed as described in B2.
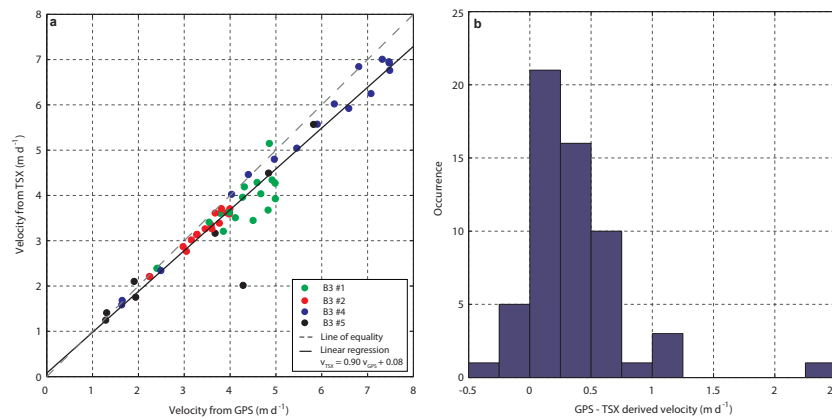
Figure A2. Comparison of TSX and GPS velocities at GPS locations and for each repeat-pass period. **(a)** Linear regression (solid black; $R^2 = 0.94$) predicts 94 % of the variance in TSX velocities ($0.14\,\mathrm{m\,d^{-1}}$). **(b)** TSX velocities typically slightly underestimate local (sub-pixel-scale) velocities measured at the GPS stations by $0.3\,\mathrm{m\,d^{-1}}$.

Appendix B: Calving flux

The calving flux, q, of Basin-3 was calculated based on TSX velocity maps and changes in the extent of the glacier by $q = q_{fg} + q_t$, with q_{fg} being the ice flux through a fluxgate near the calving front, and q_t the volume change of the terminus downglacier of that fluxgate due to advance or retreat of the calving front. Here, we defined a spatially fixed fluxgate approximately perpendicular to the ice flow, typically 1–3 km upglacier from the actual calving front (Fig. A1a), and where ice surface velocities could be inferred from all TSX-image pairs. The ice-flux can be written as

$$q_{fg} = H_{fg} \cdot w_{fg} \cdot v_{fg}, \tag{B1}$$

where $H_{fg} = zs_{fg} - zb_{fg}$ is the ice thickness along the fluxgate, with zs_{fg} and zb_{fg} the surface and bedrock elevation, respectively; w_{fg} is the width of the fluxgate; and v_{fg} the velocity across the fluxgate. We assume plug flow, i.e. depth-averaged velocities equal surface velocities, because at the high flow velocities observed, ice deformation is negligible compared to basal motion (Clarke, 1987). Position changes of the calving front are addressed by changes in areal extent of the glacier downstream from that fluxgate per repeat-pass period

$$q_t = H_t \cdot \frac{\Delta A_t}{\Delta t}, \tag{B2}$$

where $H_t = zs_t - zb_t$ is the ice thickness at the terminus in vicinity of the calving front, where zs_t represents a typical height of the calving front and zb_t is the mean bedrock elevation for the area encompassed by the observed maximum and minimum glacier extent. ΔA_t is the areal change of the terminus over the repeat-pass period Δt between successive TSX acquisitions. The uncertainty in the calving flux estimate is associated with uncertainties of the input variables listed in Table B1. If the variables are derived from several independent components, their uncertainties can be summed by the root of the sum of squares (RSS) of the uncertainty of the components.

B1 Ice flux

To calculate the ice flux $q_{fg,i}$ for each repeat-pass period t_i (Fig. 4a), the ice flux through 617 fluxgate segments 50 m in width was integrated, accounting for local ice thickness and velocity. Ice volume is converted to mass using an ice density $\rho_{ice} = 917 \, kg \, m^{-3}$. The cumulative ice flux over the period 19 April 2012 to 9 May 2013 is derived by summing up the ice flux over 19 successive TSX repeat-pass periods, weighted by their time duration (Fig. 4b):

$$q_{fg} = w_{fg} \cdot \sum_{t_i=1}^{19} \sum_{n=1}^{617} H|_{fg,n} \cdot v|_{fg,i,n} \cdot \rho_{ice}. \tag{B3}$$

To derive continuous velocity profiles along the fluxgates, the velocity maps were interpolated horizontally in the vicin-

ity of the fluxgate where mismatches occurred. The velocity maps associated with long repeat-pass periods, t_3 and t_6, suffer from large gaps: only 51 and 46 % of the fluxgate segments hold sound velocity estimates. In the case of t_3, the available data align with the previous velocity profile for t_2, a factor x relation was determined, and the gaps were filled by means of piecewise polynomial interpolation so that $v(t_3) = x \cdot v(t_2)$. In the case of t_6, the velocity profile was constructed by using the mean of the previous and following repeat-pass cycle, $v(t_6) = \frac{1}{2} \cdot (v(t_5) + v(t_7))$ (dash-dotted lines in Fig. A1a). The accuracy of the resulting velocity profiles was evaluated by comparing the constructed velocity profiles and the available reliable matches, revealing a standard deviation of 0.21 and 0.25 m d^{-1} and a negligible mean offset of 0.03 and 0.04 m d^{-1} in the case of t_3 and t_6, respectively.

The uncertainty in the ice-flux term, Δq_{fg}, is derived according to the law of propagation of uncertainty:

$$\Delta q_{fg} = w_{fg} \cdot \sum_{t_i=1}^{19} \sum_{n=1}^{617} \sigma(q_{fg})_{i,n}, \tag{B4}$$

with $\left(\frac{\sigma(q_{fg})}{q_{fg}}\right)^2 = \left(\frac{\sigma(H_{fg})}{H_{fg}}\right)^2 + \left(\frac{\sigma(v_{fg})}{v_{fg}}\right)^2$, omitting indexes i and n.

B2 Position changes of calving front

Similarly, the calving flux term related to position changes of the calving front can be expressed by the volume change of the terminus in vicinity of the calving front, q_t:

$$q_t = H_t \cdot \sum_{t_i=1}^{19} \frac{\Delta A_{t,i}}{\Delta t_i} \cdot \rho_{ice}. \tag{B5}$$

The calving front outlines of Basin-3 were digitized from geocoded TSX intensity images. Due to layover and shadow effects along the calving front a systematic error of the order of twice the height of the calving front of 30 m is assumed (Moholdt and Kääb, 2012). The digitizing accuracy is conservatively estimated to be 4 pixels, i.e. ±8 m.

Analogous to the ice-flux term, the uncertainty in the terminus-change term, Δq_t, is determined by the law of propagation of uncertainty:

$$\Delta q_t = \sum_{t_i=1}^{19} \sigma(q_t)_i \cdot \rho_{ice}. \tag{B6}$$

For each repeat-pass period, $\sigma(q_t)$ is determined by $\left(\frac{\sigma(q_t)}{q_t}\right)^2 = \left(\frac{\sigma(H_t)}{H_t}\right)^2 + \left(\frac{\sigma(\Delta A_t)}{\Delta A_t}\right)^2$, omitting index i.

Table B1. Calving flux input variables – values, sources and uncertainties.

Variable	Value/source	Uncertainty	Explanation
zs_{fg}	40 m (constant)	± 30 m	The chosen values allow for elevations from flotation height of 10 m as lower limit and mean DEM height of 67 m as upper limit. The DEM originates from prior to surge initiation. GPS data since 2008 indicate extensional flow and hence dynamic thinning.
zb_{fg}	Local bedrock map values	± 30 m	Twice the accuracy in ice thickness measurement of ± 15 m used to derive the bedrock map along fluxgate (Dunse et al., 2012), thereby accounting for uncertainties introduced by gridding of spatially inhomogeneous measurements.
H_{fg}	$zs_{fg} - zb_{fg}$	± 42 m	RSS of errors in zs_{fg} and zb_{fg}.
zs_t	30 m (constant)	± 20 m	Allows for calving front heights down to flotation and significantly larger than typical front height of 30 m (Moholdt and Kääb, 2012).
zb_t	-87 m (constant)	± 30 m	Value represents the mean bedrock elevation within the observed range in front position with an uncertainty analogous to the one of zb_{fg}.
H_t	$zs_t - zb_t$	± 36 m	RSS of errors in zs_t and zb_t.
v_{fg}	Local value from TSX velocity maps	± 0.37 m d^{-1} (0.42 for t_3 and 0.44 for t_6)	Uncertainty based on standard deviation (SD) of TSX and GPS velocities, yielding 0.37 m d^{-1}; for the long repeat cycles t_3 and t_6, additional uncertainty is added based on a comparison of the available data (51 and 46 % coverage) and reconstructed velocity profile, resulting in a SD of 0.21 and 0.25 m d^{-1}.
Front position	2 m resolution TSX backscatter image	± 8 m (4 pixels)	Digitizing error of calving front position results in uncertainty of ΔA_{cf}, determined by RSS of deviation from minimum and maximum extent of A_{cf} at times $t_{i,\text{start}}$ and $t_{i,\text{start}}$.

Appendix C: Crevasse formation

Ground-penetrating radar (GPR) profiling has been performed on Austfonna on an annual basis since spring 2004 (Dunse et al., 2009). The GPR was operated at a centre frequency of 800 MHz and provides information over a depth range of about ∼ 12 m. The data allow for identification of individual surface crevasses. Survey profiles initially focused on the accumulation area. Since 2008, the flowline along which GPS receivers are deployed has also repeatedly been surveyed. In the accumulation area, crevasse formation took place between 2004 and 2007 (Fig. C1a and b) as well as between 2008 and 2012 (Fig. C1c and d) for the western and eastern profile, respectively. The monitored flowline towards the terminus was already heavily crevassed at the time of the first GPR survey (Fig. C1c).
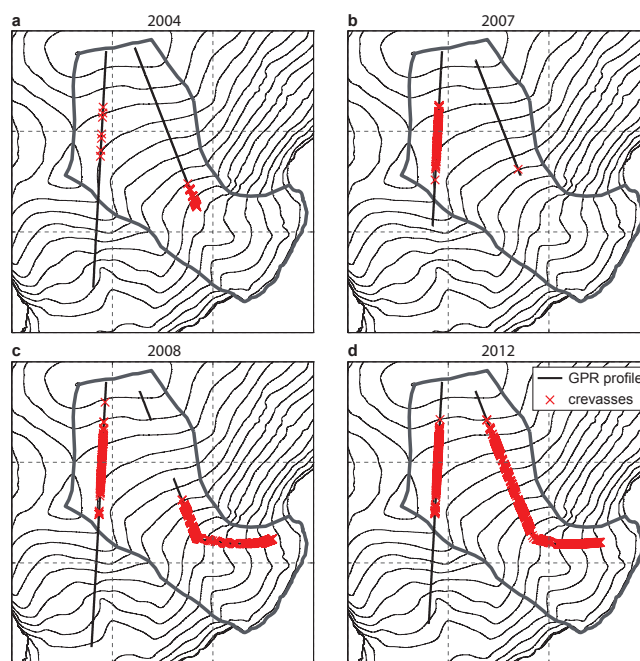
Figure C1. Crevasse formation on upper Basin-3 in 2004–2012 inferred from GPR. GPR profiles are plotted in solid black, detected crevasses are marked as red crosses. The outline of Basin-3 is shown in dark grey.
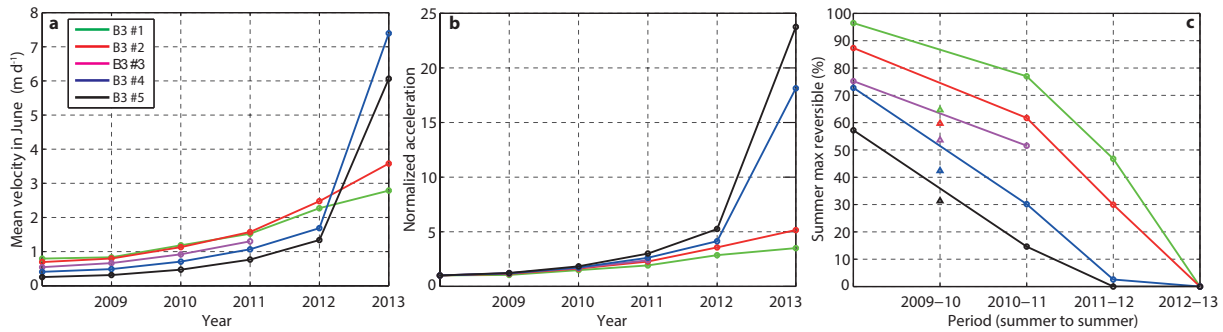
Figure D1. GPS-velocity evolution along a central flowline of Basin-3: **(a)** annual velocity minimum defined as the mean value in June 2008 to 2013 and **(b)** normalized to mean June velocity 2008, and **(c)** reversibility of summer speed-up defined as the ratio of the velocity increase from pre-summer minimum (mean June) to maximum summer velocity and subsequent velocity decrease to pre-summer velocity of the subsequent year. In 2009, summer maximum velocities were not captured due to GPS power loss. The triangles only indicate a minimum estimate for 2009–2010, based on elevated late-summer velocities measured after maintenance of GPS receivers at the end of August.

Appendix D: Background GPS velocities and summer speed-up

Our 5-year GPS record from Basin-3 shows that the annual velocity minimum typically occurs in June, just prior to the onset of summer speed-up (Dunse et al., 2012). Since 2008, the mean velocity in June has increased dramatically, with values in 2012 that were 3 to 5 times higher than in 2008 at the lowest (GPS B3 #1) and highest elevation (B3 #5), respectively (Fig. D1a and b). The strong acceleration results from flow velocities remaining above their pre-summer values after the annual summer speed-up. In particular, the reversible fraction of the summer speed-up decreases with time and diminishes in 2013, when the entire basin was surging (Fig. D1c). While the two upper GPS stations (B3 #4 and B3 #5) experience further drastic acceleration (factor of 24 and 18 increase in June 2013 compared to June 2008, respectively), the lower GPS stations (B3 #1 and B3 #2) only show moderate velocity increases, because the locations are close to the lateral shear margins of the surging basin (Fig. 3c and d).

References

Alley, R. B.: In search of ice-stream sticky spots, J. Glaciol., 39, 447–454, 1993.

Alley, R. B., Fahnestock, M., and Joughin, I.: Climate Change. Understanding Glacier Flow in Changing Times, Science, 322, 1061–1062, doi:10.1126/science.1166366, 2008.

AMAP: Snow and Water and Ice and Permafrost in the Arctic (SWIPA): Climate Change and the Cryosphere, Arctic Monitoring and Assessment Programme (AMAP), vol. xii, Oslo, Norway, 2011.

Bartholomew, I., Nienow, P., Mair, D., Hubbard, A., King, M. A., and Sole, A.: Seasonal evolution of subglacial drainage and acceleration in a Greenland outlet glacier, Nat. Geosci., 3, 408–411, doi:10.1038/NGEO863, 2010.

Bartholomew, I., Nienow, P., Sole, A., Mair, D., Cowton, T., King, M., and Palmer, S.: Seasonal variations in Greenland Ice Sheet motion: Inland extent and behaviour at higher elevations, Earth Planet. Sci. Lett., 307, 271–278, doi:10.1016/j.epsl.2011.04.014, 2011.

Bond, G., Heinrich, H., Broecker, W., Labeyrie, L., McManus, J., Andrews, J., Huon, S., Jantschik, R., Clasen, S., Simet, C., Tedesco, K., Mieczyslawa, K., Bonani, G., and Ivy, S.: Evidence For Massive Discharges of Icebergs Into the North-atlantic Ocean During the Last Glacial Period, Nature, 360, 245–249, 1992.

Church, J. A., White, N. J., Konikow, L. F., Domingues, C. M., Cogley, J. G., Rignot, E., Gregory, J. M., van den Broeke, M. R., Monaghan, A. J., and Velicogna, I.: Revisiting the Earth's sea-level and energy budgets from 1961 to 2008, Geophys. Res. Lett., 38, L18601, doi:10.1029/2011GL048794, 2011.

Clarke, G.: Thermal regulation of glacier surging, J. Glaciol., 16, 231–250, 1976.

Clarke, G.: Fast glacier flow - ice streams and surging and and tidewater glaciers, J. Geophys. Res.-Solid, 92, 8835–8841, 1987.

Clarke, G., Collins, S., and Thompson, D.: Flow and thermal structure and and subglacial conditions of a surge-type glacier, Can. J. Earth Sci., 21, 232–240, 1984.

Clason, C. C., Mair, D. W. F., Nienow, P. W., Bartholomew, I. D., Sole, A., Palmer, S., and Schwanghart, W.: Modelling the transfer of supraglacial meltwater to the bed of Leverett Glacier, southwest Greenland, The Cryosphere Discuss., 8, 4243–4280, doi:10.5194/tcd-8-4243-2014, 2014.

Comiso, J. C.: Variability and trends in Antarctic surface temperatures from in situ and satellite infrared measurements, J. Climate, 13, 1674–1696, doi:10.1175/1520-0442(2000)013<1674:VATIAS>2.0.CO;2, 2000.

Cook, C. P., van de Flierdt, T., Williams, T., Hemming, S. R., Iwai, M., Kobayashi, M., Jimenez-Espejo, F. J., Escutia, C., Jairo Gonzalez, J., Khim, B.-K., McKay, R. M., Passchier, S., Bohaty, S. M., Riesselman, C. R., Tauxe, L., Sugisaki, S., Lopez Galindo, A., Patterson, M. O., Sangiorgi, F., Pierce, E. L., and Brinkhuis, H.: Dynamic behaviour of the East Antarctic ice sheet during Pliocene warmth, Nat. Geosci., 6, 765–769, doi:10.1038/NGEO1889, 2013.

Das, S. B., Joughin, I., Behn, M. D., Howat, I. M., King, M. A., Lizarralde, D., and Bhatia, M. P.: Fracture propagation to the base of the Greenland Ice Sheet during supraglacial lake drainage, Science, 320, 778–781, doi:10.1126/science.1153360, 2008.

den Ouden, M. A. G., Reijmer, C. H., Pohjola, V., van de Wal, R. S. W., Oerlemans, J., and Boot, W.: Stand-alone single-frequency GPS ice velocity observations on Nordenskiöldbreen, Svalbard, The Cryosphere, 4, 593–604, doi:10.5194/tc-4-593-2010, 2010.

Deschamps, P., Durand, N., Bard, E., Hamelin, B., Camoin, G., Thomas, A. L., Henderson, G. M., Okuno, J., and Yokoyama, Y.: Ice-sheet collapse and sea-level rise at the Bolling warming 14 and 600 years ago, Nature, 483, 559–564, doi:10.1038/nature10902, 2012.

Dowdeswell, J.: Drainage-basin characteristics of Nordaustlandet ice caps and Svalbard, J. Glaciol., 32, 31–38, 1986.

Dowdeswell, J., Drewry, D., Cooper, A., Gorman, M., Liestøl, O., and Orheim, O.: Digital mapping of the Nordaustlandet ice caps from airborne geophysical investigations, Ann. Glaciol., 8, 51–58, 1986.

Dowdeswell, J., Hamilton, G., and Hagen, J. O.: The duration of the active phase on surge-type glaciers: contrasts between Svalbard and other regions, J. Glaciol., 37, 388–400, 1991.

Dowdeswell, J., Hodgkins, R., Nutall, A., Hagen, J. O., and Hamilton, G.: Mass-balance Change As A Control On the Frequency and Occurrence of Glacier Surges In Svalbard and Norwegian High Arctic, Geophys. Res. Lett., 22, 2909–2912, 1995.

Dowdeswell, J., Ottesen, D., Evans, J., Cofaigh, C., and Anderson, J.: Submarine glacial landforms and rates of ice-stream collapse, Geology, 36, 819–822, 2008.

Dowdeswell, J. A., Unwin, B., Nuttall, A. M., and Wingham, D. J.: Velocity structure and flow instability and mass flux on a large Arctic ice cap from satellite radar interferometry, Earth Planet. Sci. Lett., 167, 131–140, 1999.

Dunse, T., Schuler, T. V., Hagen, J. O., Eiken, T., Brandt, O., and Høgda, K.: Recent fluctuations in the extent of the firn area of Austfonna and Svalbard and inferred from GPR, Ann. Glaciol., 50, 155–162, doi:10.3189/172756409787769780, 2009.

Dunse, T., Greve, R., Schuler, T. V., and Hagen, J. O.: Permanent fast flow versus cyclic surge behaviour: numerical simulations of the Austfonna ice cap and Svalbard, J. Glaciol., 57, 247–259, 2011.

Dunse, T., Schuler, T. V., Hagen, J. O., and Reijmer, C. H.: Seasonal speed-up of two outlet glaciers of Austfonna, Svalbard, inferred from continuous GPS measurements, The Cryosphere, 6, 453–466, doi:10.5194/tc-6-453-2012, 2012.

Gardner, A. S., Moholdt, G., Wouters, B., Wolken, G. J., Burgess, D. O., Sharp, M. J., Cogley, J. G., Braun, C., and Labine, C.: Sharply increased mass loss from glaciers and ice caps in the Canadian Arctic Archipelago, Nature, 473, 357–360, doi:10.1038/nature10089, 2011.

Gardner, A. S., Moholdt, G., Cogley, J. G., Wouters, B., Arendt, A. A., Wahr, J., Berthier, E., Hock, R., Pfeffer, W. T., Kaser, G., Ligtenberg, S. R. M., Bolch, T., Sharp, M. J., Hagen, J. O., van den Broeke, M. R., and Paul, F.: A Reconciled Estimate of Glacier Contributions to Sea Level Rise: 2003 to 2009, Science, 340, 852–857, doi:10.1126/science.1234532, 2013.

Hamilton, G. S. and Dowdeswell, J. A.: Controls on glacier surging in Svalbard, J. Glaciol., 42, 157–168, 1996.

Hewitt, I.: Seasonal changes in ice sheet motion due to melt water lubrication, Earth Planet. Sci. Lett., 371–372, 16–25, doi:10.1016/j.epsl.2013.04.022, 2013.

Iken, A. and Bindschadler, R.: Combined measurements of sub-glacial water-pressure and surface velocity of Findelengletscher and Switzerland – conclusions about drainage system and sliding mechanism, J. Glaciol., 32, 101–119, 1986.

IPCC: Climate Change 2013: The Physical Science Basis, in: Contribution of Working Group I to the Fifth Assessment Report of the Intergovernmental Panel on Climate Change, edited by: Stocker, T. F., Qin, D., Plattner, G.-K., Tignor, M., Allen, S. K., Boschung, J., Nauels, A., Xia, Y., Bex, V., and Midgley, P. M., Cambridge University Press, Cambridge, UK and New York, USA, 1535 pp., doi:10.1017/CBO9781107415324, 2013.

Jiskoot, H., Murray, T., and Boyle, P.: Controls on the distribution of surge-type glaciers in Svalbard, J. Glaciol., 46, 412–422, 2000.

Joughin, I. and Alley, R. B.: Stability of the West Antarctic ice sheet in a warming world, Nat. Geosci., 4, 506–513, doi:10.1038/NGEO1194, 2011.

Joughin, I., Smith, B. E., Shean, D. E., and Floricioiu, D.: Brief Communication: Further summer speedup of Jakobshavn Isbræ, The Cryosphere, 8, 209–214, doi:10.5194/tc-8-209-2014, 2014.

Khan, S. A., Kjaer, K. H., Bevis, M., Bamber, J. L., Wahr, J., Kjeldsen, K. K., Bjork, A. A., Korsgaard, N. J., Stearns, L. A., van den Broeke, M. R., Liu, L., Larsen, N. K., and Muresan, I. S.: Sustained mass loss of the northeast Greenland ice sheet triggered by regional warming, Nat. Clim. Change, 4, 292–299, doi:10.1038/NCLIMATE2161, 2014.

Lefauconnier, B. and Hagen, J. O.: Surging and Calving Glaciers in Eastern Svalbard, Norsk Polarinstitutt, Oslo, Norway, 1991.

Luckman, A., Murray, T., and Strozzi, T.: Surface flow evolution throughout a glacier surge measured by satellite radar interferometry, Geophys. Res. Lett., 29, 10-1–10-4, doi:10.1029/2001GL014570, 2002.

Meier, M. and Post, A.: What are glacier surges, Can. J. Earth Sci., 6, 807–817, 1969.

Meier, M. and Post, A.: Fast tidewater glaciers, J. Geophys. Res.-Solid, 92, 9051–9058, 1987.

Meierbachtol, T., Harper, J., and Humphrey, N.: Basal Drainage System Response to Increasing Surface Melt on the Greenland Ice Sheet, Science, 341, 777–779, doi:10.1126/science.1235905, 2013.

Mengel, M. and Levermann, A.: Ice plug prevents irreversible discharge from East Antarctica, Nat. Clim. Change, 4, 451–455, doi:10.1038/nclimate2226, 2014.

Moholdt, G. and Kääb, A.: A new DEM of the Austfonna ice cap by combining differential SAR interferometry with ICESat laser altimetry, Polar Res., 31, 18460, doi:10.3402/polar.v31i0.18460, 2012.

Moholdt, G., Hagen, J. O., Eiken, T., and Schuler, T. V.: Geometric changes and mass balance of the Austfonna ice cap, Svalbard, The Cryosphere, 4, 21–34, doi:10.5194/tc-4-21-2010, 2010a.

Moholdt, G., Nuth, C., Hagen, J. O., and Kohler, J.: Recent elevation changes of Svalbard glaciers derived from ICESat laser altimetry, Remote Sens. Environ., 114, 2756–2767, 2010b.

Moon, T., Joughin, I., Smith, B., van den Broeke, M. R., van de Berg, W. J., Noël, B., and Usher, M.: Distinct patterns of seasonal Greenland glacier velocity, Geophys. Res. Lett., 41, 7209–7216, doi:10.1002/2014GL061836, 2014.

Mouginot, J., Rignot, E., and Scheuchl, B.: Sustained increase in ice discharge from the Amundsen Sea Embayment, West Antarctica, from 1973 to 2013, Geophys. Res. Lett., 41, 1576–1584, doi:10.1002/2013GL059069, 2014.

Murray, T., Stuart, G., Miller, P., Woodward, J., Smith, A., Porter, P., and Jiskoot, H.: Glacier surge propagation by thermal evolution at the bed, J. Geophys. Res.-Sol. Ea., 105, 13491–13507, 2000.

Murray, T., Luckman, A., Strozzi, T., and Nuttall, A. M.: The initiation of glacier surging at Fridtjovbreen and Svalbard, Ann. Glaciol., 36, 110–116, doi:10.3189/172756403781816275, 2003a.

Murray, T., Strozzi, T., Luckman, A., Jiskoot, H., and Christakos, P.: Is there a single surge mechanism? Contrasts in dynamics between glacier surges in Svalbard and other regions, J. Geophys. Res.-Sol. Ea., 108, 2237, doi:10.1029/2002JB001906, 2003b.

Nick, F., Vieli, A., Howat, I., and Joughin, I.: Large-scale changes in Greenland outlet glacier dynamics triggered at the terminus, Nat. Geosci., 2, 110–114, 2009.

Nick, F. M., Vieli, A., Andersen, M. L., Joughin, I., Payne, A., Edwards, T. L., Pattyn, F., and van de Wal, R. S. W.: Future sea-level rise from Greenland/'s main outlet glaciers in a warming climate, Nature, 497, 235–238, doi:10.1038/nature12068, 2013.

Pattyn, F.: Antarctic subglacial conditions inferred from a hybrid ice sheet/ice stream model, Earth Planet. Sci. Lett., 295, 451–461, doi:10.1016/j.epsl.2010.04.025, 2010.

Pfeffer, W. T.: A simple mechanism for irreversible tidewater glacier retreat, J. Geophys. Res.-Earth, 112, F03S25, doi:10.1029/2006JF000590, 2007.

Phillips, T., Rajaram, H., and Steffen, K.: Cryo-hydrologic warming: A potential mechanism for rapid thermal response of ice sheets, Geophys. Res. Lett., 37, L20503, doi:10.1029/2010GL044397, 2010.

Phillips, T., Rajaram, H., Colgan, W., Steffen, K., and Abdalati, W.: Evaluation of cryo-hydrologic warming as an explanation for in-

creased ice velocities in the wet snow zone and Sermeq Avan-narleq and West Greenland, J. Geophys. Res.: Earth, 118, 1241–1256, doi:10.1002/jgrf.20079, 2013.

Raymond, C.: How do glaciers surge – a review, J. Geophys. Res.-Solid, 92, 9121–9134, 1987.

Robin, G. D. Q.: Ice movement and temperature distribution in glaciers and ice sheets, J. Glaciol., 2, 589–606, 1955.

Robinson, P. and Dowdeswell, J.: Submarine landforms and the behavior of a surging ice cap since the last glacial maximum: The open-marine setting of eastern Austfonna and Svalbard, Mar. Geol., 286, 82–94, doi:10.1016/j.margeo.2011.06.004, 2011.

Schoof, C.: Ice-sheet acceleration driven by melt supply variability, Nature, 468, 803–806, doi:10.1038/nature09618, 2010.

Schuler, T. V., Dunse, T., Ostby, T. I., and Hagen, J. O.: Meteorological conditions on an Arctic ice cap-8 years of automatic weather station data from Austfonna, Svalbard, Int. J. Climatol., 34, 2047–2058, doi:10.1002/joc.3821, 2014.

Shannon, S. R., Payne, A. J., Bartholomew, I. D., van den Broeke, M. R., Edwards, T. L., Fettweis, X., Gagliardini, O., Gillet-Chaulet, F., Goelzer, H., Hoffman, M. J., Huybrechts, P., Mair, D. W. F., Nienow, P. W., Perego, M., Price, S. F., Smeets, C. J. P. P., Sole, A. J., van de Wal, R. S. W., and Zwinger, T.: Enhanced basal lubrication and the contribution of the Greenland ice sheet to future sea-level rise, P. Natl. Acad. Sci. USA, 110, 14156–14161, doi:10.1073/pnas.1212647110, 2013.

Shepherd, A., Ivins, E. R., Geruo, A., Barletta, V. R., Bentley, M. J., Bettadpur, S., Briggs, K. H., Bromwich, D. H., Forsberg, R., Galin, N., Horwath, M., Jacobs, S., Joughin, I., King, M. A., Lenaerts, J. T. M., Li, J., Ligtenberg, S. R. M., Luckman, A., Luthcke, S. B., McMillan, M., Meister, R., Milne, G., Mouginot, J., Muir, A., Nicolas, J. P., Paden, J., Payne, A. J., Pritchard, H., Rignot, E., Rott, H., Sorensen, L. S., Scambos, T. A., Scheuchl, B., Schrama, E. J. O., Smith, B., Sundal, A. V., van Angelen, J. H., van de Berg, W. J., van den Broeke, M. R., Vaughan, D. G., Velicogna, I., Wahr, J., Whitehouse, P. L., Wingham, D. J., Yi, D., Young, D., and Zwally, H. J.: A Reconciled Estimate of Ice-Sheet Mass Balance, Science, 338, 1183–1189, doi:10.1126/science.1228102, 2012.

Solheim, A.: The depositional environment of surging sub-polar tidewater glaciers: a case study of the morphology and sedimentation and sediment properties in a surgeaffected marine basin outside Nordaustlandet and the Northern Barents Sea, Skrifter – Norsk Polarinstitutt, Oslo, Norway, 194, 5–97, 1991.

Strozzi, T., Luckman, A., Murray, T., Wegmüller, U., and Werner, C. L.: Glacier motion estimation using SAR offset-tracking procedures, IEEE T. Eosci. Remote, 40, 2384–2391, 2002.

Tedesco, M., Fettweis, X., Mote, T., Wahr, J., Alexander, P., Box, J. E., and Wouters, B.: Evidence and analysis of 2012 Greenland records from spaceborne observations, a regional climate model and reanalysis data, The Cryosphere, 7, 615–630, doi:10.5194/tc-7-615-2013, 2013.

Tulaczyk, S., Kamb, W. B., and Engelhardt, H. F.: Basal mechanics of Ice Stream B and West Antarctica 2. Undrained plastic bed model, J. Geophys. Res.-Sol. Ea., 105, 483–494, 2000.

van der Veen, C.: Fundamentals of Glacier Dynamics, Taylor & Francis, the Netherlands, 472 pp., 1999.

Zagorodnov, V., Sinkevich, S., and Arkhipov, S.: Ice core express-analysis for structure and thermal regime studies of Austfonna, Data of Glaciological Studies, 66, 149–158, 1989.

Zwally, H. J., Abdalati, W., Herring, T., Larson, K., Saba, J., and Steffen, K.: Surface melt-induced acceleration of Greenland ice-sheet flow, Science, 297, 218–222, 2002.